SPACE WEATHER, VOL. 11, 476–488, doi:10.1002/swe.20071, 2013

Space weather radiation effects on geostationary satellite solid-state power amplifiers

W.Q. Lohmeyer[1] and K. Cahoy[1,2]

Received 12 April 2013; revised 8 July 2013; accepted 8 July 2013; published 27 August 2013.

[1] In order to understand and mitigate the effects of space weather on the performance of geostationary (GEO) communications satellites, we analyze 16 years of archived telemetry data from Inmarsat, the UK-based telecommunications company. We compare 665,112 operational hours of housekeeping telemetry from two generations of satellites, designated as Fleet A and Fleet B. Each generation experienced 13 solid-state power amplifier (SSPA) anomalies for a total of 26 anomalies from 1996 to 2012. We compare telemetry from the Inmarsat anomalies with space weather observations, including data from the OMNI2 database, Geostationary Operational Environmental Satellites, the Advanced Composition Explorer Satellite, and Los Alamos National Laboratory (LANL) GEO observations; the evolution of the sunspot number; and the *Kp* index. Most SSPA anomalies for Fleet A occur as solar activity declines; Fleet B has not yet experienced a full solar cycle. For both fleets, the average value of *Kp* remained < 2 over time periods of 2 days, 3 days, and 2 weeks around the time of anomaly, which suggests that the anomalies occurred at times of relatively quiet geomagnetic activity and that they were probably not solely caused by surface charging. From 1996 to 2009, the average of the 1.8–3.5 MeV electron flux was 1.98 #/(cm^2 s st keV). Five of the 26 anomalies, unfortunately, do not have corresponding science observations (specifically, electron flux data in the LANL data set), so part of this study focuses on the 21 anomalies when science observations were available. Six out of 21 anomalies experienced a high-energy electron flux greater than 1.5 standard deviations above the mean of the $\log_{10}$ of the flux between 7 and 14 days prior to the anomaly. By contrast, a Monte Carlo simulation finds that on average, only 2.8 out of 21 (13%) of randomly assigned "anomalies" occur between 7 and 14 days after an electron flux greater than 1.5 standard deviations above the mean. Our observations suggest that internal charging from either past elevated radiation belt fluxes or some conditions related to relativistic electron enhancements (either causally or accidentally) is most likely responsible for the SSPA anomalies. We next consider the timing of these anomalies with respect to the local time (LT) and season. Anomalies occur at all LT sectors with 46% (Fleet A) and 38.5% (Fleet B) in the midnight to dawn sector and 54% (Fleet A) and 46% (Fleet B) in the local noon to dusk sector. From the local time distribution, surface charging does not appear to be the sole causative agent of the anomalies. Understanding the connection between the space weather conditions and anomalies on subsystems and specific components on identical and similar geostationary communications satellites for periods of time longer than a solar cycle will help guide design improvements and provide insight on their operation during space weather events.

Citation: Lohmeyer, W. Q., and K. Cahoy (2013), Space weather radiation effects on geostationary satellite solid-state power amplifiers, *Space Weather*, *11*, 476–488, doi:10.1002/swe.20071.

[1]Department of Aeronautics and Astronautics, Massachusetts Institute of Technology, Cambridge, Massachusetts, USA.
[2]Department of Earth, Atmospheric, and Planetary Sciences, Massachusetts Institute of Technology, Cambridge, Massachusetts, USA.

Corresponding author: W. Q. Lohmeyer, Department of Aeronautics and Astronautics, Massachusetts Institute of Technology, Cambridge, MA 02139, USA. (whitneylohmeyer@gmail.com)

1542-7390/13/10.1002/swe.20071

1. Introduction

[2] Space weather can impact the performance of satellite systems and can cause satellite anomalies [e.g., *Baker*, 2000; *Fennell et al.*, 2001; *Iucci et al.*, 2006; *Allen*, 2010]. However, the ability to quantify these effects requires a statistical analysis of both space weather and satellite anomaly data, along with an increased understanding of the space environment and specific information about the affected systems and their accommodation on the spacecraft [*Baker*, 2002; *Tretkoff*, 2010]. Observations of the space

environment covering complete solar cycles are currently more widely available than satellite health data and information on anomaly occurrences, which is quite limited.

[3] Recently, *Choi et al*. [2011] have analyzed the effects of space weather on 95 satellite anomalies from 79 unique satellites archived in the Satellite News Digest between 1997 and 2009. The study noted relationships between anomalies and seasonal dependencies, satellite local time, geomagnetic index *Kp*, and charged particles observed by Los Alamos National Laboratory (LANL) satellites but did not find any dependency on solar cycle. The study suggested that energetic electrons might contribute to anomalies but noted that the relationship between anomalies and electrons is not well established. *Mazur and O'Brien* [2012] commented on the data population of *Choi et al*. [2011] and emphasized the importance of a careful analysis of the anomaly records. Further, *Thomsen et al*. [2013] analyzed the statistical properties of the surface-charging environment at geostationary orbit and found statistical evidence in support of the *Choi et al*. [2011] conclusions and also determined that an increased probability of surface charging exists during the declining phase of the solar cycle, when the probability of internal charging from relativistic electrons is also elevated.

[4] The purpose of this analysis is to improve the understanding of the effects of space weather on geostationary satellites while focusing on specific types of component anomalies that have multiple occurrences in similar systems. We collaborate with Inmarsat, a telecommunications company based in the UK, to analyze 665,112 operational hours of satellite telemetry data from eight satellites on two of the Inmarsat's satellite fleets. There are five satellites in what we will call Fleet A and three satellites in Fleet B. Analyzing data from five satellites of the same fleet and then comparing the results with a second three-satellite fleet provide insight into both how space weather affects similar components and systems within each fleet as well as general trends that are common for different fleets. Such an approach is only possible within a focused study and cannot be applied to a more general statistical analysis of different spacecraft anomalies.

[5] In order to more accurately quantify the effect of space weather on geostationary communications satellites, we focus on one type of component anomaly, those affecting solid-state power amplifiers (SSPAs). Power amplifiers are a critical component in all radio frequency satellite communication systems: They amplify the uplink signals received by the satellite from the ground before retransmitting the downlink signals to the users on the ground [*Strauss*, 1993]. The satellite communications industry uses both SSPAs and traveling wave tube amplifiers (TWTAs) as power amplifiers. While TWTAs currently have efficiency advantages for higher-power wideband applications, SSPAs require a lower voltage and have advantages in size and weight [*Sechi and Bujatti*, 2009].

[6] Since 1996, the eight Inmarsat satellites have experienced 26 solid-state power amplifier (SSPA) anomalies; individually, each satellite has experienced between zero and eight SSPA anomalies. SSPAs consist of an electrical power conditioner (EPC) and field effect transistors (usually gallium arsenide (GaAs)). Operators classify the SSPA anomalies into two categories: "hard" failures and "soft" failures. Soft failures are when amplifiers experience low current conditions, but are recoverable. Hard failures are not recoverable and may even lead to a temporary bus power shutdown on the spacecraft. Both types of failures are identified when spacecraft health telemetry, such as the SSPA current used in this work, falls below a predefined threshold. The threshold setting is specific to particular hardware; for example, the SSPA current thresholds for Fleet A SSPAs and Fleet B SSPAs are different because the configurations, manufacturers, and/or model of these components are different. The spacecraft health measurements are continuously recorded (e.g., hourly) and saved and then downlinked to the ground where they are monitored and archived. SSPA anomalies have occurred as early in a satellite's lifetime as in the first 3 months of operation and as late as nearly 15 years of operation. All known SSPA anomalies present in the Inmarsat archive for these two fleets are considered in this study; none were removed. There is no identified or confirmed cause for any of the 26 anomalies, and thus, they are considered to be "random" failures [e.g., *Weekley and Mangus*, 2005]. Due to the fact that satellites are not returned to Earth for anomaly investigation, the actual cause of the individual SSPA anomalies is challenging to diagnose [*Thomsen et al*., 2013; *Choi et al*., 2011; *Baker*, 2000]. However, the effects of high-energy particle radiation from relativistic electrons, low-energy electrons, and high-energy protons, as well as galactic cosmic rays, are suspected to play a major role [*Baker*, 2000].

[7] In this work, we compare 26 total SSPA anomalies with observations of the space weather environment. Specifically, we compare the SSPA telemetry at the time of the anomaly to high-energy relativistic electrons and low-energy electrons. Five of the 26 anomalies unfortunately do not have corresponding science observations (specifically, electron flux data in the LANL data set), so part of this study focuses on the 21 anomalies when science observations were available. The Inmarsat archives used in this work contain the following information for eight geostationary (GEO) satellites: SSPA telemetry (current and temperature), eclipse data, and SSPA anomaly information for eight spacecraft from 1996 to 2012. The complete telemetry data archives are a treasure trove of combined science and engineering information on commercial communication components' response to space weather and contain valuable information about how space weather impacts flight electronics and materials as a function of age, time, and location.

[8] The overall purpose of this paper is to investigate whether space weather effects are the likely cause of SSPA anomalies and which effects and causes of failure are the most likely candidates. Our preliminary analysis, for most of the SSPA anomalies, does not support an association between the SSPA anomalies and energetic solar proton events, solar flares, or strong ring current (large negative

Dst) events [*Lohmeyer et al*., 2012]. Therefore, similar to the study conducted by *Choi et al*. [2011], here we investigate relationships between anomalies and geomagnetic index *Kp* in section 3.1, high-energy electrons in section 3.2, magnetic local time in section 3.3, and seasonal dependencies in section 3.4.

[9] We also analyze hazardous particle populations that may affect the SSPA components on the geostationary satellites, including low-energy electrons, which can cause surface charging, and high-energy relativistic electrons, which can cause internal charging. Spacecraft charging occurs when surrounding plasma particles bombard the satellite and can deposit charge onto the surface of the satellite or even penetrate the satellite shielding and deposit in the internal components. Once a buildup of charge accumulates beyond the material's breakdown potential, an electrostatic discharge (ESD) occurs and impulsively emits energy that can cause single event upsets (SEUs) or component anomalies in electronic systems [*Fennell et al*., 2001; *Baker*, 2002; *Bodeau*, 2010]. As previously mentioned, in future work, we will analyze galactic cosmic rays, which can cause anomalies and single event upsets [*Baker*, 2000].

[10] The OMNI2 data set is the primary data set used in this study and was obtained from the Goddard Space Flight Center/Space Physics Data Facility OMNIWeb interface at http://web.gsfc.nasa.gov. OMNI2 contains hourly measurements of near-Earth solar wind magnetic field and plasma parameters, as well as the *Kp* index, the disturbance storm time (*Dst*) index, auroral electrojet (*AE*), and proton flux values. The OMNI2 data come from numerous satellites, such as the Advanced Composition Explorer (ACE) satellite, the International Monitoring Platform satellites, and the Geostationary Operational Environmental Satellite (GOES), as well as from the Data Analysis Center for Geomagnetism and Space Magnetism at Kyoto University in Japan [*King and Papitashvili*, 2004]. High-energy electron flux data (1.8–3.5 and 3.5–6 MeV) were obtained from the Los Alamos National Laboratory (LANL) geosynchronous charged particle instruments [*Reeves et al*., 2011].

[11] In this work, we also use the energetic particle data (2 MeV electron flux) from the GOES satellite that is longitudinally closest to the respective Inmarsat satellite that experienced the anomaly. The closest GOES satellite is located within 60° of longitude from the Inmarsat satellite for 15 of the 26 anomalies. The farthest separation between a GOES satellite and an Inmarsat satellite was for two of the SSPA anomalies, when the closest GOES satellite was located 160° from the Inmarsat satellite. Interpretation of results should keep these longitudinal separations in consideration.

[12] The analysis of anomalies together with space weather data will help bring together the commercial satellite communications industry and space weather science communities to understand the sensitivity of key components to the changes of the space environment [*O'Brien et al*., 2013]. The goal is to improve both component robustness as well as system performance using design redundancy, operational, and predictive monitoring approaches.

2. Solid-State Power Amplifier (SSPA) Anomalies

[13] Throughout a spacecraft's lifetime, component health and performance degrade as a result of exposure to space weather [*Baker*, 2000]. Satellite performance anomalies occur when a component operates outside of its defined threshold for nominal performance. Thresholds are established to monitor the health of components and notify operators when the component experiences anomalous performance. For SSPAs, the main threshold of concern is the amplifier current. The SSPA current reflects the amplification capability of the device.

[14] If the amplifier current exceeds the upper threshold, the SSPA will saturate. The nonlinear amplification past saturation is undesirable as it generates harmonics and distorts the transmitted signal. If the current falls below the lower threshold, then the SSPA will not provide enough current to adequately amplify the signal. Space weather effects can modify the operation and efficiency of the amplifiers and cause amplifier anomalies, which, in turn, will limit the operational lifetime of the satellite. *Weekley and Mangus* [2005] noted that 80% of SSPA failures disable downlink capabilities. We concur that space weather can affect efficiency and satellite operational lifetime. Redundancy in design and operational management can reduce these impacts on overall performance, and in this work, we seek to improve our understanding of the space weather sensitivity and failure mechanisms.

2.1. Severity of Amplifier Anomalies

[15] Over an undetermined period of time, continuous bombardment of energetic particles can deposit themselves into an amplifier's material and change the charge mobility that was originally determined by the dopant concentrations of an amplifier's material and, thus, leads to a change in conductivity that will affect current, which is a parameter monitored and tracked in housekeeping telemetry. Similar to the two studies presented in *Strauss* [1993], the SSPAs did not experience a single generic amplifier failure mechanism but experienced abrupt unexpected switch-offs. These studies did not consider failure mechanisms associated with the space environment. Specific failure mechanisms with respect to the space environment that we investigate are surface charging caused from low-energy electrons (section 3.1) and deep dielectric charging from high-energy electrons (section 3.2).

[16] When the amplifier is irradiated by high-energy particles that transfer more than the radiation ionization energy to the semiconductor, an electron hole pair forms in the semiconductor material (such as silicon or gallium arsenide, (GaAs)) [e.g., *Alig et al*., 1975]. This changes the charge carrying capability and affects the amplification properties of the transistor of the amplifier, which can cause anomalies to occur [*Bhat et al*., 2005].

[17] Of the 26 SSPA anomalies, only 4 were soft failures, and 22 were hard failures. Only one of the SSPAs that experienced a soft failure was ultimately able to continue

nominal operation. Thus, 25/26 SSPA anomalies called for a redundant SSPA unit to be switched on. One of the 26 SSPA anomalies that called for a redundant SSPA unit did not have a replacement SSPA available because it had already been switched on from a previous anomaly. It is clear that major performance degradation results when replacement SSPAs are unavailable if they are already in use.

[18] The shielding and the mounting location of the satellite hardware play an important role in protecting components from the harmful effects of the space environment [*Strauss*, 1993]. SSPA units are generally mounted inside the satellite in an electronics box or chassis, where they can be monitored in a thermally controlled environment (thermal management of power amplifiers is a substantial part of communications satellite design). The SSPAs are also somewhat protected from space weather hazards via the external shielding of the spacecraft bus and shielding from other internal units. The typical shielding of a geostationary communications satellite is approximately 10 mil Al equivalent (or 0.254 mm of Al) for its solar arrays, which, typically, are deployed panels [*O'Brien*, 2009], and the internal shielding of SSPAs in communications satellites typically ranges between less than 1 mm Al equivalent to slightly more than 3 mm Al equivalent depending on the geometric distribution of the internal components. However, high-energy relativistic electrons ($>$ 2 MeV) and galactic particles are capable of penetrating both types of shielding and can cause anomalies for internal components [*Hastings and Garret*, 1996]. As mentioned in section 1, SSPAs consist of an RF amplifier and an electronic power conditioner (EPC). Depending on the application (orbit and expected lifetime), the devices may require spot shielding. Manufacturers perform ray tracing to quantify the amounts of shielding provided to individual components and their potential exposure to the radiation environment [*Schwank et al.*, 2008]. In the event that spot shielding is required, precautions regarding component grounding are also taken. Satellite manufacturers measure grounding as a part of assembly, integration, and testing.

[19] Due to the relatively high amounts of shielding used and the location of the SSPAs (deep within the spacecraft), we do not consider charging from substorm-injected electrons, which cause surface charging, as a primary issue for these SSPA units. However, in section 3.2, we still investigate surface charging as a potential component hazard in this study.

[20] It is relevant to note that Inmarsat has not had any extended service interruptions due to the SSPA anomalies. Satellite manufacturers incorporate redundancy into their designs, so that when an SSPA anomaly occurs, a redundant SSPA is turned on to provide continuous operation at full capacity. However, as satellite lifetimes extend beyond design expectancies, which is becoming increasingly common and is also a profitable position to be in, there are fewer available redundant units with time, and thus, satellites operating beyond their design lifetime may have more frequent outages.

[21] In the study of *Weekley and Mangus* [2005], 944 SSPAs in operation onboard 104 satellites between 1980 and 2004 were considered. Only 20% of the satellites experienced SSPA anomalies, and 9% of the satellites experienced more than two SSPA anomalies. Therefore, it was concluded that a single failure has little impact on the overall communications satellite functionality. The eight Inmarsat satellites analyzed in this study are collectively equipped with more than 450 SSPAs. Of these 450 SSPAs, 88% of the satellites we consider experienced SSPA anomalies, and 75% experienced two or more anomalies. Given the design margins in place, the systems are currently capable of absorbing the rate of SSPA anomalies [*Weekley* and *Mangus*, 2005], but we are concerned with the fact that as technological capabilities evolve (e.g., with smaller feature sizes), the susceptibility of newer technologies to radiation will also increase [*Baker*, 2000; *Love et al.*, 2000].

3. Space Weather Effects on Satellite Anomalies

[22] With the exception of galactic cosmic rays (GCRs), space weather originates from the Sun, which emits solar flares and coronal mass ejections (CMEs), and produces corotating interaction regions (CIRs) that drive high-speed solar winds. When these disturbances reach Earth, they can produce geomagnetic storms capable of causing hazardous anomalies (noise or even loss in telemetry, degradation to solar arrays, electrical upsets, etc.) and can also drastically diminish the quality of science data [e.g., *Baker*, 2002; *Cole*, 2003; *Barbieri and Mahmot*, 2004].

[23] CMEs and CIRs uniquely alter the space environment but, together, are the primary sources of geomagnetic storms [*Kamide et al.*, 1998]. CMEs result from the eruptions of the solar flares and usually occur more frequently during solar maximum [*Wilkinson*, 1994], whereas CIRs form in response to fast solar wind interacting with slower solar wind and often show a 27 day periodicity [e.g., *Denton et al.*, 2006; *Tsurutani et al.*, 1995]. CIRs are associated with high-speed solar wind, which tend to occur during the declining phase of the solar cycle, when the majority of internal charging anomalies at GEO occur [*Wrenn and Smith*, 1996]. These storms are usually longer in time, are associated with fluctuations in solar wind *Bz* component of the magnetic field, and are usually associated with the strongest increases in high-energy electrons in the outer radiation belt [*Li et al.*, 2005; *Miyoshi and Kataoka*, 2008]. Further, these relativistic electrons produce higher levels of deep dielectric charging than CMEs [*Denton et al.*, 2006].

[24] The sunspot number, a metric derived from the observations of individual sunspots and groups of sunspots, is used to assess the overall strength and variability of solar activity. The increase and decrease in the sunspot number define the maximum and minimum of the solar magnetic activity cycle, a period of approximately 11 years. At solar maximum, there is an increased chance of solar flares and CMEs, yet even at solar minimum, the Sun can produce damaging storms [*Allen*, 2010; *Cole*, 2003; *Baker*, 2000].

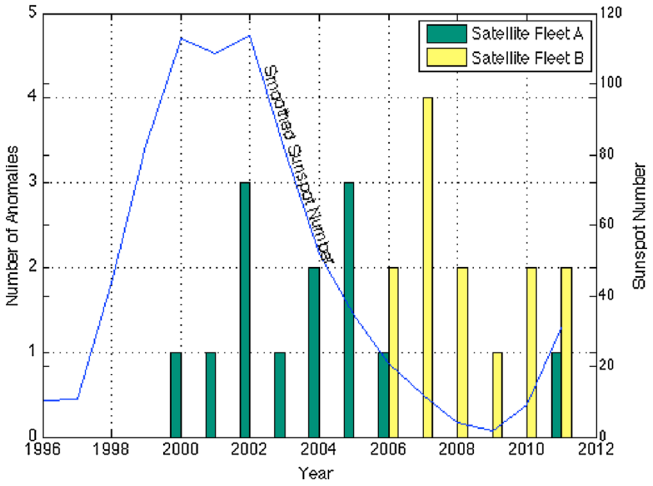

Figure 1. Yearly SSPA anomaly totals per satellite fleet, plotted with the smoothed sunspot number (blue line).

In the commercial communications world, the challenge in predicting the effect of space weather events on communications satellites leads operators to continue nominal operation during periods of increased solar activity [*O'Brien et al.*, 2013].

[25] Figure 1 displays the smoothed sunspot number from Solar Influences Data Analysis Center of the Royal Observatory of Belgium (data available at http://sidc.oma.be/sunspot-data/) and the Inmarsat SSPA anomalies between 1996 and 2012. The two satellite fleets, Fleet A and Fleet B, are designated with different colors. This period encompasses part of solar cycle 23 (May 1996 to December 2008) and part of solar cycle 24 (January 2009 to present). The solar minimum for cycle 23 occurred in 1996, and the maximum for cycle 23 occurred in 2002. The solar minimum for cycle 24 occurred between 2008 and 2009; however, the solar maximum has yet to occur for cycle 24 [*Riley*, 2012].

[26] It is important to consider the effects of space weather on Fleet A and Fleet B as they are from different satellite manufacturers. This is because different components, geometries, shielding, and operational configurations will have different sensitivities to space weather. We can compare "identical" spacecraft within Fleet A and Fleet B but here refrain from drawing conclusions using combined data over a solar cycle. Rather, we should wait until we have enough data such that each fleet has individually experienced a full solar cycle.

[27] There were no SSPA anomalies for either fleet prior to 2000, even though this time period includes launch and the initial years of operation for several of the satellites. For Fleet A, anomalies occur between 3.5 and 14.5 years of operation, whereas for Fleet B, anomalies occur from less than 0.2–7 years of operation. Therefore, the occurrence of the SSPA anomalies does not show a clear correlation with the satellite or amplifier age. It is interesting to also note that in Figure 1, Fleet A has far fewer SSPA anomalies around solar minimum than Fleet B does; this emphasizes the point that they should be considered on a fleet-by-fleet basis.

[28] Figure 2 displays the number of SSPA anomalies per year per satellite in Fleet A, along with the solar cycle. A similar graph for Fleet B is not shown because data for a full solar cycle do not exist.

[29] For Fleet A, no SSPA anomalies occur immediately after launch or even within the first 3 years of operation. The SSPA anomalies on Fleet A do not primarily occur at solar maximum, when CME-driven storms are most likely [*Denton et al.*, 2006], but occur during the declining phase of the solar cycle. As previously mentioned, the declining phase of the solar cycle is the time when CIRs drive high-speed solar wind streams and produce enhancements of relativistic electrons, notoriously known to cause internal charging [*Shea and Smart*, 1998; *Wrenn et al.*, 2002; *Denton et al.*, 2006; *Miyoshi and Kataoka*, 2008]. Hot electron temperature, which has been found to determine surface-charging levels, also reaches a maximum during the declining phase of the solar cycle [*Denton et al.*, 2006].

[30] The distribution of the 13 SSPA anomalies aboard Fleet A and the expected internal charging from energetic electrons may indicate that the anomalies were caused from surface charging from low-energy electrons or deep dielectric charging from relativistic electrons. It is still difficult to completely rule out other causes of anomalies, as there are limited statistical data. More statistical studies with space weather data over a solar cycle will be required to validate the observed correlation and definitively establish the relationship between deep dielectric charging and SSPA anomalies.

3.1. Low-Energy Electrons, Surface Charging, and the *Kp* Index

[31] Low-energy electrons, on the orders of 10 s of keV, originate in the inner magnetosphere from magnetotail

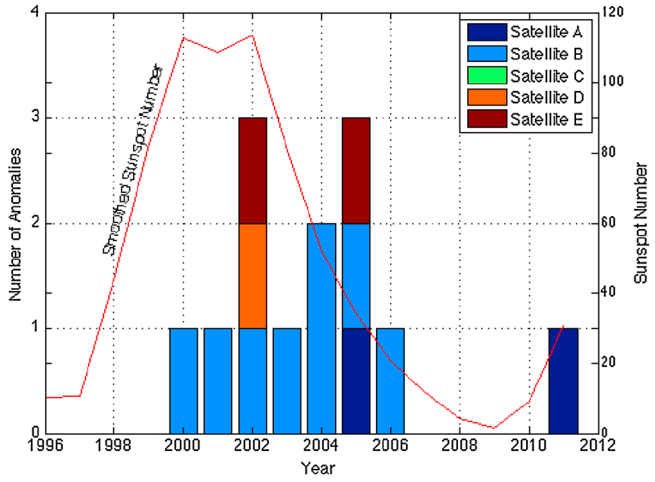

Figure 2. SSPA anomalies per year for Fleet A from 1996 to 2012. Each letter in the legend corresponds to a different satellite in the fleet. This satellite fleet has data for an entire solar cycle, whereas Fleet B has none.

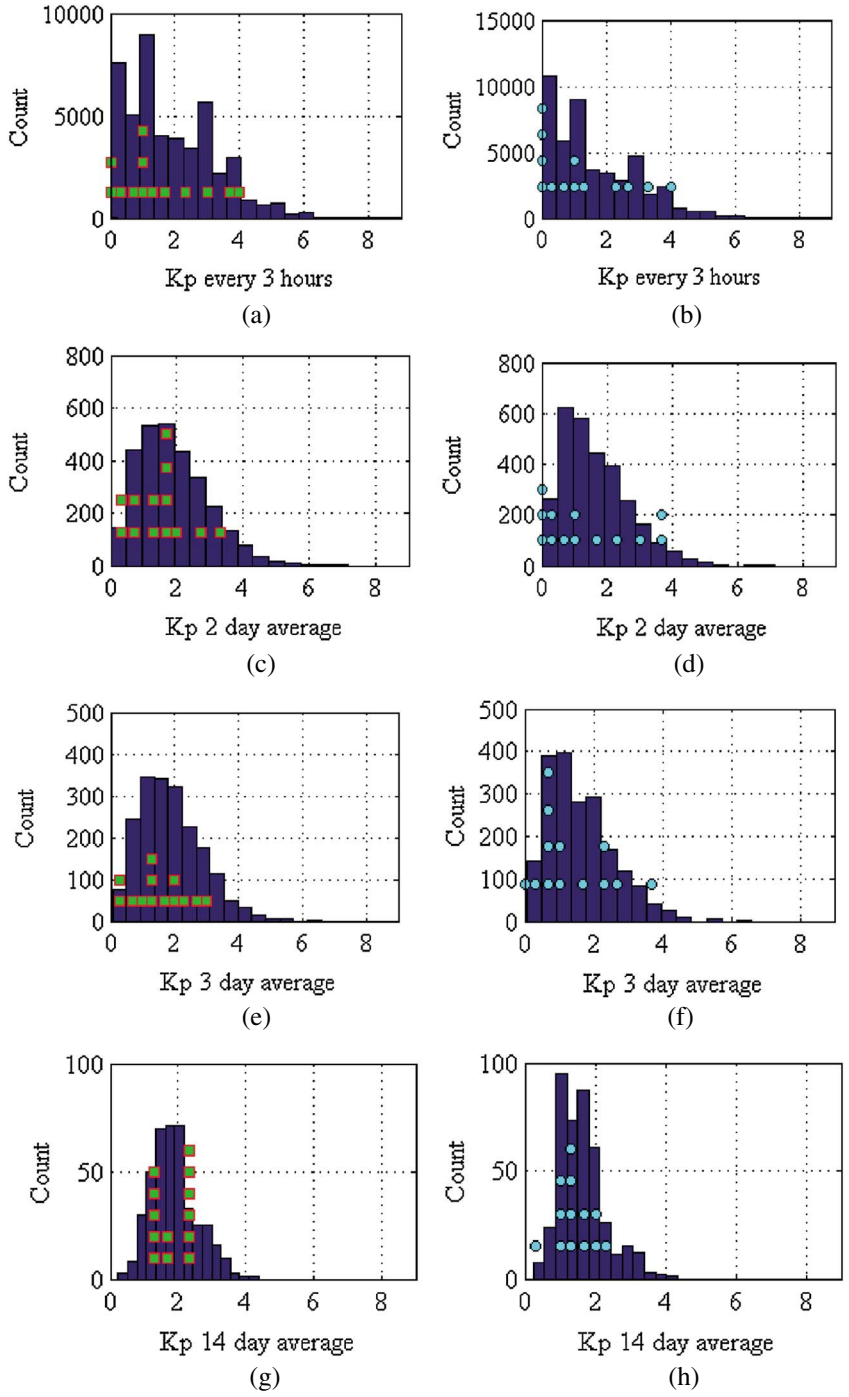

Figure 3. The distribution of the *Kp* index: (a, b) every measurement, (c, d) 2 day average, (e, f) 3 day average, and (g, h) 2 week average with the *Kp* index at the time of the SSPA anomalies. The distributions for the time period of operations of Fleet A are shown in Figures 3a, 3c, 3e, and 3g; and the anomalies of Fleet A are represented with green squares. The distributions for the time of period of operations of Fleet B are shown in Figures 3b, 3d, 3f, and 3h; and the anomalies of Fleet B are represented with cyan circles. The specific time periods of each fleet are not distinguished for proprietary reasons but only include periods when the respective satellite fleets were in operation. The *Kp* time series are taken from the Data Analysis Center for Geomagnetism and Space Magnetism at Kyoto University in Japan and was accessed through the OMNI2 website.

Table 1. Fleet A Summary of *Kp* at Time of 13 SSPA Anomalies

Fleet A	*Kp*	*Kp* 2 Day Average	*Kp* 3 Day Average	*Kp* 14 Day Average
Mean	1.538	1.542	1.567	1.848
Standard deviation	1.335	0.832	0.828	0.425
Minimum value	0	0	0.449	1.287
Maximum value	4	3.248	3.097	2.326

injections and drift eastward from the night portion of the magnetosphere [e.g., *Wrenn*, 1995; *Allen*, 2010, and references therein]. The strongest injections are produced by substorms. These particles deposit on the surface of the satellite but do not possess enough energy to penetrate shielding materials. Several geostationary satellites have experienced anomalies due to surface charging; for example, the Maritime European Communications Satellite A experienced an uncommanded switching anomaly from a sudden increase in moderate-energy electrons [*Wrenn*, 1995; *Baker*, 2000]. Furthermore, it is widely acknowledged that surface charging anomalies generally occur between local midnight and dawn [e.g., *Wrenn*, 1995; *Fennell et al*. 2001; *Lanzerotti et al*., 1998; *Allen*, 2010]. The local time (LT) analysis of the 26 SSPA anomalies is presented in section 3.3.

[32] The *Kp* magnetic disturbance index is often used as a proxy to quantify the relationship between surface charging and magnetospheric convection [*Thomsen*, 2004] that causes hot electron enhancements near geostationary orbit [e.g., *Fennell et al*., 2001; *O'Brien*, 2009; *Korth et al*., 1999]. Between 1996 and 2012, only 2.2% of the *Kp* measurements were recorded as greater than a *Kp* of 5, or as severe geomagnetic activity. However, *Denton and Borovsky* [2012, Appendix A] found that surface charging still occurs even at relatively low *Kp* values (*Kp* of approximately 2 or 3).

[33] Figures 3a–3h show the distribution of the *Kp* index from 1996 to 2012 for every *Kp* measurement (Figures 3a and 3b), *Kp* averaged over 2 days (Figures 3c and 3d), *Kp* averaged over 3 days (Figures 3e and 3f), and *Kp* averaged over 2 weeks, or 14 days (Figures 3g and 3h). The *y* axis, labeled count, represents the number of *Kp* measurements. The *Kp* distributions for Fleet A are shown in Figures 3a, 3c, 3e, and 3g. Each Fleet A anomaly is shown with a green square. The *Kp* distributions for Fleet B are shown in Figures 3b, 3d, 3f, and 3h. Each Fleet B anomaly is shown with a cyan circle. The anomaly placement points are calculated using the respective averaging method of each figure. For example, the anomaly points on Figure 3c represent the average *Kp* value of the 2 days prior to the anomaly. Each point represents a single anomaly. The vertical location of the point does not correspond to a count value, as labeled on the *y* axis of each plot.

[34] The anomalies do not appear to depend on the *Kp* index. Figure 3f, for example, shows more anomalies at small *Kp* values, and there appear to be more days with smaller *Kp* during the time of the operation of fleet B. However, after normalizing results by the number of days in the time series with a given *Kp* value, we found that anomalies do not preferentially occur for high *Kp* or low *Kp* values. Additional anomaly data will be required to verify this preliminary conclusion. A summary of the four *Kp* distributions is provided in Table 1 for Fleet A and Table 2 for Fleet B. Interestingly, for both fleets, the maximum *Kp* at the time of anomaly did not exceed a *Kp* of 4. Twenty-one out the 26 (80%) anomalies occurred when the *Kp* was less than 2.5.

[35] Tables 1 and 2 summarize the mean *Kp*, the standard deviation of the *Kp* distributions, the minimum *Kp*, and the maximum *Kp* for all four distributions. For Fleet A, the average *Kp* of all anomalies for the four distributions is greater than the respective values for Fleet B, as the anomalies of Fleet B occur after 2006 when geomagnetic activity was low. The minimum and maximum *Kp* values at the time of the anomalies are approximately equal for both fleets.

[36] To relate these results to charging phenomena, *O'Brien* [2009] found the probability of an anomaly caused by surface charging peaks in the *Kp* of 4–6 range. Similarly, *Thomsen et al*. [2013] found an increased probability of surface charging at higher *Kp* values. However, *Denton and Borovsky* [2012] found strong surface charging even at relatively low *Kp* ($> \sim 2$ or 3). We find that these specific anomalies occurred at times of quiet geomagnetic activity and are not likely caused by surface charging alone.

3.2. High-Energy Electrons and Internal Charging

[37] Most commonly, 2 MeV electron flux is used as the representative electron population capable of penetrating spacecraft structures [e.g., *Love et al*., 2000]. These relativistic electrons are accelerated during geomagnetic storms and deposit into the dielectric materials of the satellites (semiconductors and circuit boards). If the rate of charge buildup exceeds the rate at which charge can escape from the internal components, an ESD or arcing will occur [e.g., *Shea and Smart*, 1998; *Baker*, 2000; *Fennell et al*., 2001; *Bodeau*, 2010; *Lai*, 2012].

[38] The anomalies on ANIK E1, ANIK E2, the Japanese BS-3a satellite, Intelsat K, Galaxy 4, and Telstar 401 have been attributed by several previous studies to internal charging [*Baker*, 2000; *Love et al*., 2000; *Allen*, 2010; *Horne et al*., 2013]. However, at the time of the ANIK and Telstar anomalies, the 2 MeV electron flux was very weak [*Baker*, 2000]. However, some of these anomalies, such as those on the Japanese BS-3a and the ANIK satellites, did experience periods of

Table 2. Fleet B Summary of *Kp* at Time of 13 SSPA Anomalies

Fleet B	*Kp*	*Kp* 2 Day Average	*Kp* 3 Day Average	*Kp* 14 Day Average
Mean	1.277	1.427	1.387	1.406
Standard deviation	1.371	1.320	1.110	0.540
Minimum value	0	0.072	0.138	0.256
Maximum value	4	3.656	3.776	2.386

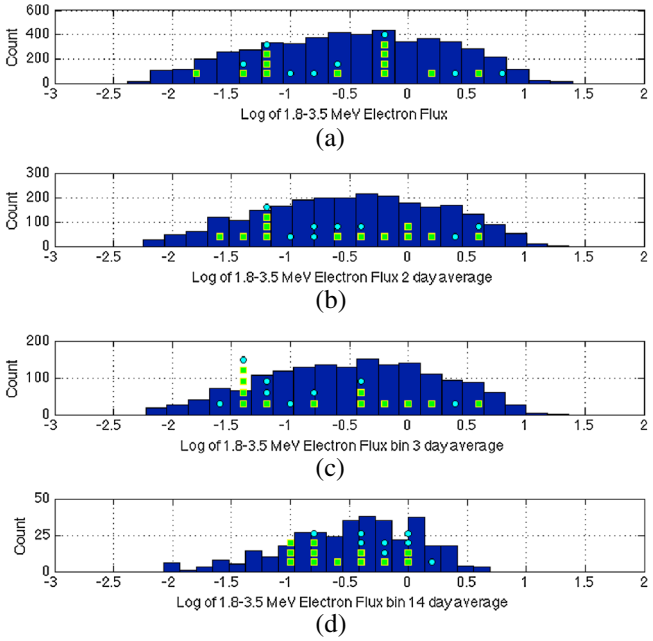

Figure 4. The distribution of the $\log_{10}$ of 1.8–3.5 MeV electron fluxes in units of #/(cm^2 s st keV) from 1996 to 2009 for (a) every 1 day average measurement, (b) 2 day average, (c) 3 day average, and (d) 2 week average with electron flux at the time of the SSPA anomalies on (green squares) Fleet A and (cyan circles) Fleet B.

high flux levels of energetic electrons 1–2 weeks before the anomalies occurred [*Shea and Smart*, 1998; *Love et al.*, 2000].

[39] Figures 4a–4d show the distribution of the $\log_{10}$ of 1.8–3.5 MeV daily averaged electron flux from 1996 to 2009 measured on the LANL Synchronous Orbit Particle Analyzer [*Reeves et al.*, 2011] for every measurement (Figure 4a), averaged over 2 days (Figure 4b), averaged over 3 days (Figure 4c), and averaged over 2 weeks, or 14 days (Figure 4d). The distribution of the $\log_{10}$ of 1.8–3.5 MeV electron flux at the time of the anomaly, approximated to the nearest 0.2 pfu (pfu = (#/(cm^2 s sr keV)), is shown for Fleet A with green squares and Fleet B with cyan circles. These points represent the $\log_{10}$ (1.8–3.5 MeV electron flux) value averaged to the same extent of the respective distribution.

[40] Similar to Figure 3, the y axis count represents the number of measurements. For these data, the measurements are daily electron flux values. The vertical location of the anomaly markers does not correspond to the count values on the y axis. For Fleet B, six anomalies occurred when flux data from LANL are not available; therefore, only 20 points are shown in Figures 4a–4d. Both fleets are shown on the same figure, rather than separated, which should be done for large data sets.

[41] From 1996 to 2009, the average $\log_{10}$ of 1.8–3.5 MeV electron flux was −0.49 $\log_{10}$ (#/(cm^2 s sr keV)) with a standard deviation of 0.75 $\log_{10}$ (#/(cm^2 s sr keV)). SSPA anomalies occur between $\log_{10}$ of electron flux values of −1.81 to 0.55 $\log_{10}$ (#/(cm^2 s sr keV)) for Fleet A and −1.47 to 0.85 $\log_{10}$(#/(cm^2 s sr keV)) for Fleet B. There does not appear to be an obvious, unique distribution of the electron flux at the time of the anomalies. However, more satellite anomaly data will help clarify if a trend exists.

[42] Since it is very difficult to evaluate the existence of elevated electron flux using a 14 day average, Figure 5a shows the 21 individual $\log_{10}$ of 1.8–3.5 MeV electron flux curves, in gray, for a period of 3 weeks before the anomaly and the curve of the daily average $\log_{10}$ of 1.8–3.5 MeV electron flux during this period. Only 21 of the 26 anomalies occur in periods when LANL 1.8 – e.5 MeV electron flux data exist. Figure 5b shows the same curve of the daily average $\log_{10}$ of 1.8–3.5 MeV electron flux 21 days before the anomalies, but with a different vertical scale. A peak in electron flux occurs between 7 and 14 days before the SSPA anomalies. Figures 5a and 5b also suggest that either past elevated radiation-belt fluxes or some conditions related to relativistic electron enhancements (either causally or accidentally) are most likely responsible for the SSPA anomalies.

[43] Although this is not shown in Figure 4, 6 of the 21 anomalies, or ~29%, experienced a flux level greater than 1.5 standard deviation above the mean $\log_{10}$ of 1.8–3.5 MeV electron flux from 1996 to 2009, or a $\log_{10}$ of 1.8–3.5 MeV electron flux of 0.64 between 7 and 14 days before the anomaly. For the entire period between 1996 and 2009, 365 out of 5110 days experienced a $\log_{10}$ of 1.8–3.5 MeV electron flux greater than 1.5 standard deviations above the mean (note that 365 days here is not related to a calendar year). From the LANL data set, 5110 days were evenly divided into 365 consecutive 14 day intervals with an imaginary "anomaly" on the last day of each 14 day interval (the 365 number of 14 day intervals is also a coincidence and has nothing to do with the days in a year). Of these 365 fourteen day intervals, 78 of them, or 21%, had daily average values greater than 1.5 standard deviations between days 7 and 14 before an anomaly.

[44] To understand the likelihood that a *random* anomaly occurs between 7 and 14 days after the level of the $\log_{10}$ of 1.8–3.5 MeV electron flux exceeds the mean by 1.5 standard deviations between 1996 and 2009, we conducted a Monte Carlo simulation. Specifically, we determined the likelihood that 21 random anomalies would occur between 7 and 14 days after a level of the $\log_{10}$ of 1.8–3.5 MeV electron flux that exceeds the mean by 1.5 standard deviations above the mean. For 100,000 iterations of the Monte Carlo simulation, we found that 2.8 out of 21, or ~13%, anomalies occur 7–14 days after a $\log_{10}$ of 1.8–3.5 MeV electron flux greater than 1.5 standard deviations above the mean. With the Monte Carlo approach, instead of the uniform distribution approach, we find that nearly twice as many (29%) anomalies occurred after elevated electron events above 1.5 standard deviations in the data as compared with the Monte Carlo trial (13%).

[45] As previously mentioned, the Japanese BS-3a and the ANIK satellites also experienced enhanced levels of high-energy electron flux 1–2 weeks before an anomaly. *Wrenn* [1995] provided statistical, conclusive evidence that internal dielectric charging was the cause of the ANIK satellite failures. Therefore, one plausible cause of these 11 SSPA

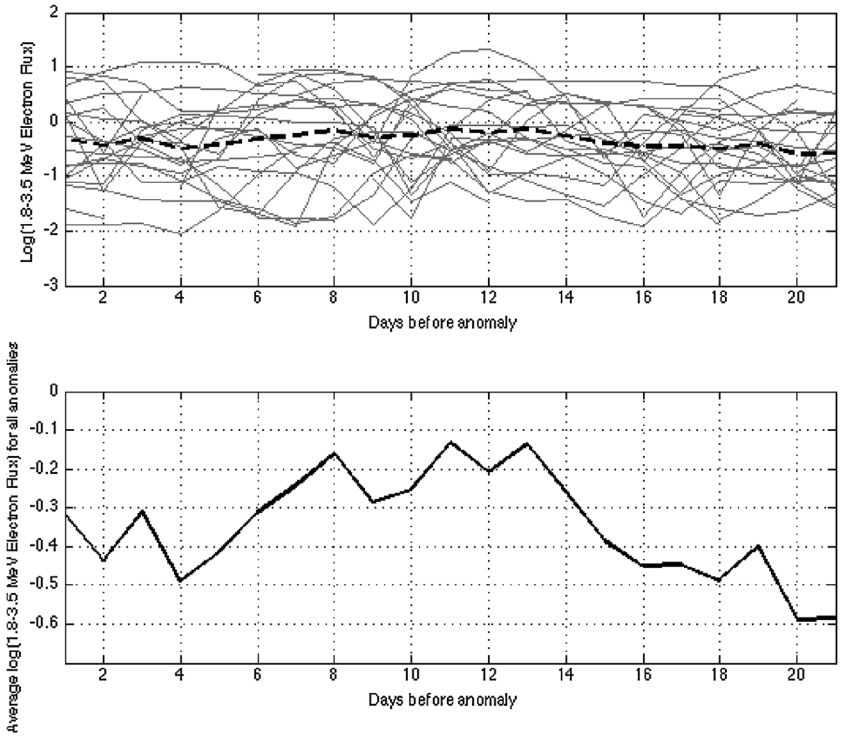

Figure 5. (a, b) Twenty-one individual $\log_{10}$ (1.8–3.5 MeV electron flux) 0–21 days before the SSPA anomalies, represented by the thin gray curves, and the daily average shown in the dashed black curve in Figure 5a. Figure 5b shows the same average $\log_{10}$ (1.8–3.5 MeV electron flux) 0–21 days before the SSPA anomalies, as shown in black in Figure 5a, but with higher resolution.

anomalies could be from internal dielectric charging. *Bodeau* [2010], however, suggests that long delays between electron enhancements and anomalies due to internal charging may not be likely. In future work, we will continue to investigate whether anomalies result from the combined effect of internal charging by comparing additional anomalies with high-energy particle populations, including GCRs.

[46] While space weather data are becoming increasingly more available, it still remains challenging to conduct analysis of satellite failures and definitively determine a cause of a single anomaly. It is interesting to have the opportunity to utilize spacecraft telemetry to understand the effects of the space weather environment, as comparing like anomalies with environmental data enables pattern identification and the establishment of a plausible cause [*Wrenn*, 1995].

[47] Figures 6a–6d display the GOES 2 MeV electron flux rate (solid blue line) and the SSPA current (dotted green line) 2 weeks before and after four SSPA anomalies. The anomaly is designated with a red line. The periodic higher-frequency variability in both the SSPA and the 2 MeV data is due to the diurnal cycle.

[48] Figure 6, as well as Figures 5a and 5b, clearly shows that there is often a drastic increase of 2 MeV electron flux that occurs approximately 1–2 weeks before the selected anomalies. The number of days between the peak 2 MeV electron flux and the four anomalies in Figures 6a–6d is 10.6 days for Figure 6a, 10.4 days for Figure 6b, 7.8 days for Figure 6c, and 10.4 days for Figure 6d.

3.3. SSPA Anomalies and Local Time

[49] Numerous studies [e.g., *Wilkinson*, 1994; *Fennell et al*., 2001; *Iucci et al*., 2006; *Choi et al*., 2011] suggest that satellite anomalies from surface charging effects depend on satellite local time, as surface charging anomalies generally tend to occur between midnight and dawn. Internal charging often occurs at times near local noon but can also occur outside of this time sector [*Fennell et al*., 2001; *Wrenn et al*., 2002]. *Choi et al*. [2011] found that for 95 GEO anomalies, 72% of the anomalies occur between midnight and dawn in local time. In *Choi et al*. [2011], the anomalies are not only SSPAs but also include a variety of additional failures.

[50] In Figure 7, we plot the local time of each of the 26 SSPA anomalies on the eight Inmarsat satellites. Fleet A is represented with red circles, and Fleet B is shown in black asterisks. The radial distance from the center of the graph has no significance but is used for clarity since several anomalies occur at similar local times.

[51] Of the 13 SSPA anomalies in Fleet A, six (46%) occurred around local midnight, and the remaining seven (54%) occurred more loosely around local noon (one each closer to the dawn and dusk sectors than to local noon). For Fleet B, five of the thirteen occur in the approximately

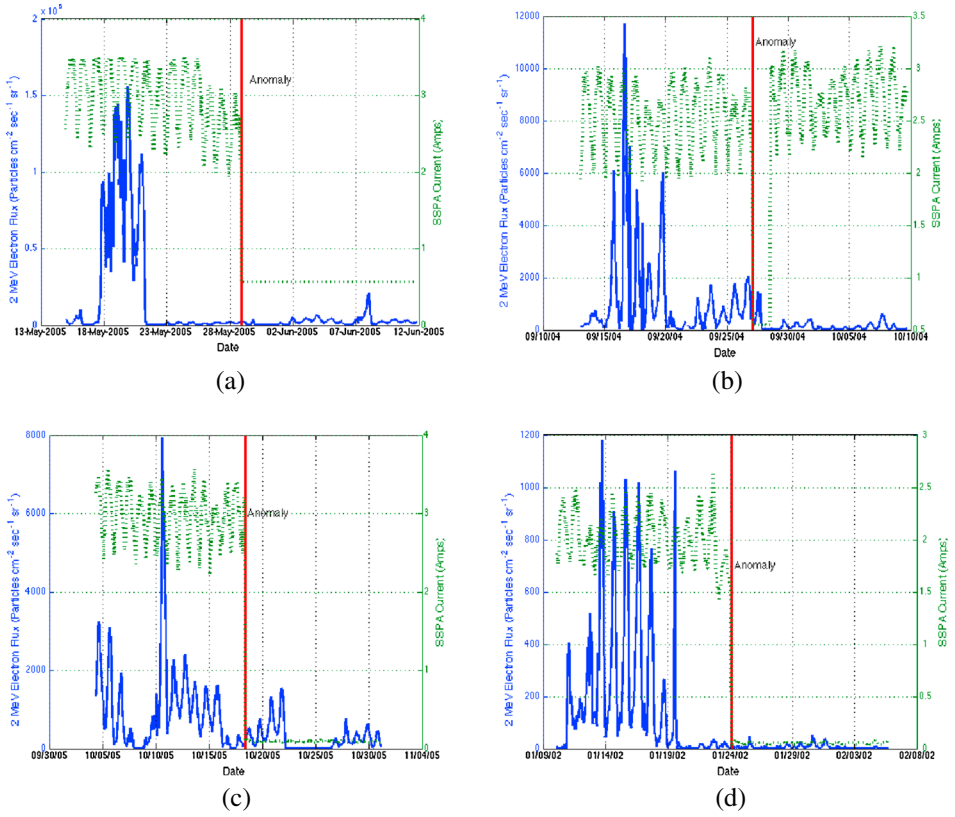

Figure 6. (a–d) Two MeV electron flux during SSPA anomaly for 2 weeks before and after four anomalies. GOES 2 MeV electron flux is plotted on the left vertical axis, and SSPA current is plotted on the right axis. The GOES 2 MeV electron flux is the blue line, the SSPA current is the dotted green line, and the anomaly is marked with a red line. The higher-frequency variability in both electron flux and current is due to the diurnal cycle.

midnight to dawn sector (38.5%), and six (46%) occur in the local noon to dusk sector. *Thomsen et al*. [2013] showed that there is essentially zero chance that anomalies between 12 and 17 local time (LT) are caused from surface charging. Seven of the 26 anomalies occur between 12 and 17 LT and are thus not considered to have resulted from surface charging. The local time distribution of the Inmarsat anomalies indicates that surface charging could not have been the causative agent for all of the SSPA anomalies.

3.4. SSPA Anomalies and Eclipse Data

[52] In the event of an eclipse, the Earth blocks sunlight from reaching the solar arrays and requires satellite operators to monitor and control power use. The two eclipse seasons are late February to mid-April (spring eclipse season) and late August to late October (fall eclipse season). The longest eclipses generally last between 68 and 73 min [*Lohmeyer et al*., 2012]. The eclipse seasons coincide with the vernal and autumnal equinox, because it is during

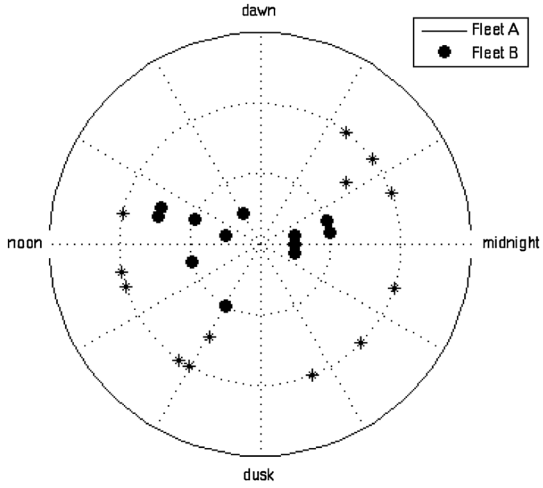

Figure 7. Local time for the 26 SSPA anomalies onboard (red circles) Fleet A and (black asterisk) Fleet B. The radial distance from the center of the plot is an offset for clarity and has no other significance.

Table 3. The Number of SSPA Anomalies per Season on Each of the Inmarsat Satellites[a]

Satellite	Winter	Spring	Summer	Fall
A	1	1	0	0
B	1	3	0	4
C	0	0	1	0
D	2	0	0	0
E	2	1	1	1
F	1	2	1	2
G	1	0	0	1
Total	8	7	3	8

[a]Only seven of the satellites are tabulated, as one satellite did not experience any SSPA anomalies.

equinox that the Earth blocks the Sun's light from reaching the satellites.

[53] *Choi et al*. [2011] found that more of the geostationary satellite anomalies occurred in spring (March, April, and May) and fall (September, October, and November) than in summer and winter. Spring and fall are known as periods when geomagnetic activity is at a maximum [*Russell and McPherron*, 1973]. However, despite there being an observed semiannual variation in geomagnetic activity as well as in GEO anomalies [*Wilkinson*, 1994; *Iucci et al*, 2006], this result was not observed for the 26 SSPA anomalies on board the Inmarsat satellites. Table 3 shows the season in which each of the 26 SSPA anomalies occur. The specific satellite longitudes are kept anonymous to respect proprietary information.

[54] No obvious seasonal trend for the anomalies exists. More than half of the anomalies (16/26) occurred in winter and fall, and the fewest number of anomalies occurred in summer. Interestingly, January was the month with the most anomalies, but is a time when geomagnetic activity is at a minimum [*Russell and McPherron*, 1973]. One possible explanation of these results is that the geometry of the Earth eclipsing the Sun, in addition to the measures taken by the operators during eclipse seasons for power management, seems to reduce the number of SSPA anomalies. However, the local time distribution presented in section 3.3 suggests that an eclipse effect is rather unlikely. Additional anomaly data would help determine if these types of components are susceptible to the previously noted seasonal dependencies of geostationary anomalies [*Iucci et al*., 2006; *Wilkinson*, 1994; *Choi et al*., 2011].

4. Summary and Discussions

[55] We analyze the 26 SSPA anomalies experienced on eight Inmarsat satellites between 1996 and 2012. The SSPA anomalies occurred between launch and 15 years of operation. We compare the SSPA telemetry at the time of the anomaly to low-energy electrons and high-energy relativistic electrons to understand if the anomalies were likely due to surface charging or deep dielectric charging, respectively.

[56] Based on the Inmarsat SSPA data alone, we cannot generalize that all geostationary communications satellite anomalies have a causal relationship with the sunspot cycle (11 year solar cycle). More Fleet A SSPA anomalies occur during the declining phase of the solar cycle, when relativistic electron fluxes reach their highest values, but also when surface charging is most likely to occur [*Thomsen et al*., 2013].

4.1. Surface Charging Discussion

[57] To understand the relationship of the SSPA anomalies and surface charging, the *Kp* index was analyzed. The anomalies do not appear to have a clear relationship with the *Kp*. Twenty-one out of the 26 (80%) anomalies occurred when the *Kp* was less than 2.5 at the time of the anomaly, and all 26 (100%) of the anomalies occurred with a 2 week average *Kp* value of less than 2.5. This suggests that the anomalies occurred at times of relatively quiet geomagnetic activity and that the anomalies are likely not caused by surface charging. It should be noted that relativistic electron fluxes, which are discussed in more detail below, are often weaker during the time of low *Kp*.

[58] Furthermore, 7 of the 26 SSPA anomalies occur at a local time between 12 and 17 LT when surface charging is not likely to occur [*Thomsen et al*., 2013]. More anomalies occur in the noon to dusk sector (54% for Fleet A and 46% for Fleet B) than at the midnight to dawn local time sector (46% and 38.5%). The frequency of occurrence is slightly less at midnight, which indicates that other space weather effects than surface charging play a role.

4.2. Deep Dielectric Charging Discussion

[59] The second space weather–related failure mechanism considered is internal charging caused from high-energy electrons. While most of the anomalies occurred during the declining phase of the solar cycle, when electron fluxes are enhanced, there does not appear to be an obvious relationship between the anomalies and 1.8–3.5 MeV electron fluxes at the time of anomaly or prior to the anomaly. However, 6 of the 21 anomalies, nearly 30% of the anomalies, experienced electron flux greater than 1.5 standard deviations of the long-term average electron flux approximately 1–2 weeks prior to the anomaly. For a uniform distribution of anomalies over 5110 days of LANL electron flux data (in 365 fourteen day intervals with an imaginary anomaly at the end of each interval), we find 78/365 of the 14 day intervals, or 21%, had events with daily average electron flux values above 1.5 standard deviations from days 7 to 14 of each interval. For 21 anomalies randomly distributed across the 5110 days, with 100,000 iterations of the Monte Carlo simulation described in section 3.2, we found that 2.8 out of a random set of 21 anomalies, or 13%, would occur 7–14 days after a $\log_{10}$ of 1.8–3.5 MeV electron flux greater than 1.5 standard deviations above the mean.

[60] Other satellites, such as the Japanese BS-3a and the ANIK satellites, have experienced enhanced levels of high-energy electron flux 1–2 weeks before an anomaly as well. One potential explanation could be a combined effect of relativistic electrons and galactic cosmic rays. GCRs probability also increase as solar cycle declines. In the future, analysis of the relationship of GCRs and the SSPA anomalies will be conducted. Furthermore, as *Wrenn*

[1995] suggested, internal dielectric charging sensors for GEO satellites are useful for monitoring the high-energy electron flux at the declining phase of the solar cycle and would help monitor and potentially predict the occurrence of major operational anomalies from internal charging.

[61] Additionally, we considered the occurrence rate of SSPA anomalies with geostationary eclipse season (during the equinoxes). No obvious seasonal distribution exists, yet more than half of the anomalies (16/26) occur in winter and fall. However, the month with the highest number of anomalies is January, when geomagnetic activity is typically low [*Russell and McPherron*, 1973].

[62] While space weather data are becoming increasingly more available, it still remains challenging to conduct analyses of anomaly failures using both space weather data and satellite telemetry. This study uniquely utilizes spacecraft telemetry to understand the effects of the space weather environment. Contributions to anomalies may also come from other factors such as the date from the launch, the age of the satellite, the time the SSPA started being operational, and the type of satellite. Additional SSPA anomaly data, as well as additional space weather observations, will improve our understanding of the correlation between spacecraft anomalies and the space weather environment.

[63] **Acknowledgments.** We thank Inmarsat and the NSF (W.Q. Lohmeyer is an NSF graduate fellow) for supporting this work. We would like to acknowledge Yuri Shprits for his contributions and feedback, Adam Kellerman for his assistance with data processing, and Geoff D. Reeves for providing LANL data in *Reeves et al*. [2011]. We would also like to acknowledge Mark Dickinson, Marcus Vilaca, the Inmarsat Spacecraft Analysts, Jacob Bortnik, Daniel Baker, Michelle Thomsen, Janet Green, Cathryn Mitchell, Paul T. O'Brien, Joseph Kinrade, the Invert Centre for Imaging Science at the University of Bath, Gregory Ginet, Anthea Coster, Trey Cade, and Fred DeJarnette for their input and guidance. We thank NASA (OMNI2), NOAA, LANL, ACE, SIDC, and the World Data Center for Geomagnetism for access to their space environment databases.

References

Alig, R. C., and S. Bloom (1975), Electron-hole-pair creation energies in semiconductors, *Phys. Rev. Lett.*, *35*(22), 1522–1524, doi:10.1103/PhysRevLett.35.1522.

Allen, J. (2010), The Galaxy 15 anomaly: Another satellite in the wrong place at a critical time, *Space Weather*, *8*, S06008, doi:10.1029/2010SW000588.

Baker, D. N. (2000), The occurrence of operational anomalies in spacecraft and their relationship to space weather, *IEEE Trans. Plasma Sci.*, *28*(6), 2007–2016, doi:10.1109/27.902228.

Baker, D. N. (2002), How to cope with space weather, *Science*, *297*(5586), 1486–1487, doi:10.1126/science.1074956.

Barbieri, L. P., and R. E. Mahmot (2004), October-November 2003's space weather and operations lessons learned, *Space Weather*, *2*, S09002, doi:10.1029/2004SW000064.

Bhat, R. B., N. Upadhyaya, and R. Kulkarni (2005), Total radiation dose at geostationary orbit, *IEEE Trans. Nucl. Sci.*, *52*(2), 530–534.

Bodeau, M. (2010), High energy electron climatology that supports deep charging risk in GEO, paper presented at 48th AIAA Aerospace Sciences Meeting Including the New Horizons Forum and Aerospace Exposition, Orlando, Fla., 4–7 January.

Choi, H. S., J. Lee, K. S. Cho, Y. S. Kwak, I. H. Cho, Y. D. Park, Y. H. Kim, D. N. Baker, G. D. Reeves, and D. K. Lee (2011), Analysis of GEO spacecraft anomalies: Space weather relationships, *Space Weather*, *9*, S06001, doi:10.1029/2010SW000597.

Cole, D. G. (2003), Space weather: Its effects and predictability, *Space Sci. Rev.*, *107*, 295–302, doi:10.1007/978-94-007-1069-6_27.

Denton, M. H., and J. E. Borovsky (2012), Magnetosphere response to high-speed solar wind streams: A comparison of weak and strong driving and the importance of extended periods of fast solar wind, *J. Geophys. Res.*, *117*, A00L05, doi:10.1029/2011JA017124.

Denton, M. H., J. E. Borovsky, R. M. Skoug, M. F. Thomsen, B. Lavraud, M. G. Henderson, R. L. McPherron, J. C. Zhang, and M. W. Liemohn (2006), Geomagnetic storms driven by ICME and CIR-dominated solar wind, *J. Geophys. Res.*, *111*, A07S07, doi:10.1029/2004JA011436.

Fennell, J. F., H. C. Koons, J. L. Roeder, and J. B. Blake (2001), Spacecraft charging: Observations and relationships to satellite anomalies, *Aerosp. Rep. TR-2001(8570)-5*, Aerosp. Corp., Los Angeles, Calif.

Hastings, D., and H. Garret (1996), *Spacecraft-Environment Interactions*, Cambridge Univ. Press, New York.

Horne, R. B., S. A. Glauert, N. P. Meredith, D. Boscher, V. Maget, D. Heynderickx, and D. Pitchford (2013), Space weather impacts on satellite and forecasting the Earth's electron radiation belts with 2 SPACECAST, *Space Weather*, *11*, 169–186, doi:10.1002/swe.20023.

Iucci, N., et al. (2006), Spacecraft operational anomalies and space weather impact hazards, *Adv. Space Res.*, *37*, 184–190, doi:10.1016/j.asr.2005.03.028.

Kamide, Y., et al. (1998), Current understanding of magnetic storms: Storm-substorm relationships, *J. Geophys. Res.*, *103*(A8), 17705–17728, doi:10.1029/98JA01426.

King, J. H., and N. E. Papitashvili (2004), Solar wind spatial scales in and comparisons of hourly wind and ACE plasma and magnetic field data, *J. Geophys. Res.*, *110*, A02209, doi:10.1029/2004JA010804.

Korth, H., M. F. Thomsen, J. E. Borovsky, and D. J. McComas (1999), Plasma sheet access to geosynchronous orbit, *J. Geophys. Res.*, *104*, 25,047–25,061.

Lai, S. (2012), *Fundamentals of Spacecraft Charging*, Princeton Univ. Press, Princeton, N. J.

Lanzerotti, L. J., C. Breglia, D. W. Maurer, G. K. Johnson III, and C. G. Maclennan (1998), Studies of spacecraft charging on geosynchronous telecommunications satellite, *Adv. Space Res.*, *22*, doi:10.1016/SO273-1177(97)01104-6.

Li, X., D. N. Baker, M. Temerin, G. Reeves, R. Friedel, and C. Shen (2005), Energetic electrons, 50 keV to 6 MeV at geosynchronous orbit: Their responses to solar wind variations, *Space Weather*, *3*, S04001, doi:10.1029/2004SW000105.

Lohmeyer, W., K. Cahoy, and D. N. Baker (2012), Correlation of GEO communication satellite anomalies and space weather phenomena: Improved satellite performance and risk mitigation, paper presented at 30th AIAA International Communications Satellite Systems Conference (ICSSC), Ottawa, Canada.

Love, D. P., D. S. Toomb, D. C. Wilkinson, and J. B. Parkinson (2000), Penetrating electron fluctuations associated with GEO spacecraft anomalies, *IEEE Trans. Plasma Sci.*, *28*, 2075–2084, doi:10.1109/27.902234.

Mazur, J. E., and T. P. O'Brien (2012), Comment on "Analysis of GEO spacecraft anomalies: Space weather relationships" by Ho-Sung Choi et al, *Space Weather*, *10*, S03003, doi:10.1029/2011SW000738.

Miyoshi, Y., and R. Kataoka (2008), Flux enhancement of the outer radiation belt electrons after the arrival of stream interaction regions, *J. Geophys. Res.*, *113*, A03S09, doi:10.1029/2007JA012506.

O'Brien, T. P., J. E. Mazur, and J. F. Fennell (2013), The priority mismatch between space science and satellite operations, *Space Weather*, *11*, 49, doi:10.1002/swe.20028.

O'Brien, T. P. (2009), SEAES-GEO: A spacecraft environmental anomalies expert system for geosynchronous orbit, *Space Weather*, *7*, S09003, doi:10.1029/2009SW000473.

Reeves, G. D., S. K. Morley, R. H. W. Friedel, M. G. Henderson, T. E. Cayton, G. Cunningham, J. B. Blake, R. A. Christensen, and D. Thomsen (2011), On the relationship between relativistic electron flux and solar wind velocity: Paulikas and Blake revisited, *J. Geophys. Res.*, *116*, A02213, doi:10.1029/2010JA015735.

Riley, P. (2012), On the probability of occurrence of extreme space weather events, *Space Weather*, *10*, SO2012, doi:10.1029/2011SW000734.

Russell, C. T., and R. L. McPherron (1973), Semiannual variation of geomagnetic activity, *J. Geophys. Res.*, *78*(1), 92–108, doi:10.1029/JA078i001p00092.

Schwank, J. R., M. R. Shaneyfelt, and P. E. Dodd (2008), Radiation hardness assurance testing of microelectronic devices and

integrated circuits: Radiation environments, physical mechanisms, and foundations for hardness assurance, *Sandia Natl. Lab. Doc.* SAND-2008-6851P, Albuquerque, New Mexico.

Sechi, F., and M. Bujatti (2009), *Solid-State Microwave High-Power Amplifiers*, Artech House, Norwood, Mass.

Shea, M. A., and D. F. Smart (1998), Space weather: The effects on operations in space, *Adv. Space Res.*, *22*(1), 29–38, doi:10.1016/S0273-1177(97)01097-1.

Strauss, R. (1993), Orbital performance of communication satellite microwave power amplifiers (MPAs), *Int. J. Satell. Commun.*, *11*, 279–285, doi:10.1002/sat.4600110506.

Thomsen, M. F. (2004), Why *Kp* is such a good measure of magnetospheric convection, *Space Weather*, *2*, S11004, doi:10.1029/2004SW000089.

Thomsen, M. F., M. G. Henderson, and V. K. Jordanova (2013), Statistical properties of the surface-charging environment at geosynchronous orbit, *Space Weather*, *11*, 237–244, doi:10.1002/swe.20049.

Tretkoff, E. (2010), Space weather and satellite engineering: An interview with Michael Bodeau, *Space Weather*, *8*, SO3003, doi:10.1029/2010SW000584.

Tsurutani, B., W. D. Gonzalez, A. L. C. Gonzalez, F. Tang, J. K. Arballo, and M. Okada (1995), Interplanetary origin of geomagnetic activity in the declining phase of the solar cycle, *J. Geophys. Res.*, *100*, 21717, doi:10.1029/95JA01476.

Weekley, J. M., and B. J. Mangus (2005), TWTA versus SSPA: A Comparison of on-orbit reliability data, *IEEE Trans. Electron Devices*, *52*(5), 650–652, doi:10.1109/TED.2005.845864.

Wilkinson, D. C. (1994), National Oceanic and Atmospheric Administration's spacecraft anomaly data base and examples of solar activity affecting spacecraft, *J. Spacecr. Rockets*, *31*, 160–165, doi:10.2514/3.26417.

Wrenn, G. L. (1995), Conclusive evidence for internal dielectric charging anomalies on geosynchronous communications spacecraft, *J. Spacecr. Rockets*, *32*(3), 514–520, doi:10.2514/3.26645.

Wrenn, G. L., and R. J. K. Smith (1996), Probability factors governing ESD effects in geosynchronous orbit, *IEEE Trans. Nucl. Sci.*, *42*(6), 2783–2789, doi:10.1109/23.556867.

Wrenn, G. L., D. J. Rodgers, and K. A. Ryden (2002), A solar cycle of spacecraft anomalies due to internal charging, *Ann. Geophys.*, *20*(7), 953–956, doi:10.5194/angeo-20-953-2002.